

Development of the Nano Hummingbird: A Tailless Flapping Wing Micro Air Vehicle

Matthew Keenon,¹ Karl Klingebiel,² Henry Won,³ and Alexander Andriukov⁴
AeroVironment Inc., Simi Valley, CA, 93065

This paper describes the development and design of the Nano Hummingbird, a small hovering ornithopter, which was developed as a part of the Defense Advanced Research Projects Agency (DARPA) Nano Air Vehicle (NAV) program. Announced in 2005, the NAV program goal was defined as a small, biologically inspired, unmanned air vehicle that would sustain hover and fly forward up to 10 m/s, while having a size under 7.5 cm, a total mass under 10g, and a payload of 2g. In 2011, the Nano Hummingbird was unveiled by AeroVironment as the culmination of over four years of work by a small team of engineers, technicians, artists, and modelers. It had a mass of 19 g, a wingspan of 16.5 cm, and the ability to hover for several minutes, fly forward up to 6.7 m/s, and transmit live color video to a remote ground station. Additionally, the vehicle demonstrated the ability to perform controlled hovering flight strictly with the use of its two flapping wings, a feat that was previously only seen in nature. The first part of this paper describes the history of the program, the evolution of the flying prototypes, and highlights the performance and characteristics of the flight vehicle. In the second part, further detailed explanation of the design of the subsystems is provided – including the flapping mechanism, control mechanism, wings, and onboard avionics – and their own paths of development.

I. Introduction

THE Nano Air Vehicle (NAV) program was announced in a 2005 Broad Agency Announcement (BAA)¹ by the Defense Advanced Research Projects Agency (DARPA), with the goal of developing unmanned air vehicle (UAV) systems no larger than 7.5 cm in any dimension, and having a gross takeoff weight (GTOW) of 10 g or less while carrying a 2 g payload. Notional mission performance requirements included range greater than 1000 m, the ability to hover in place for 60 seconds or more, slow and fast forward speeds of 0.5 and 5-10 m/s, close quarter navigation, and controlled payload drop capability. The vehicle was to be teleoperated from a ground control station, but not required to operate fully autonomously. While not strictly required, minimal visual and acoustic signatures, as well as stealth by mimicry were highly desired.

In response to the DARPA request, AeroVironment proposed to build a two-winged, free flying, flapping wing micro air vehicle. The team's basic goals were for the vehicle to be wirelessly piloted remotely through downlinked onboard video, provide roll, pitch, yaw, and thrust controls comparable to a helicopter (Fig. 1), and mimic the appearance and flight characteristics of biological hummingbirds. It was envisioned that these goals would be best accomplished by an electric powered vehicle, carrying its own rechargeable battery energy source, utilizing a conventional DC electric propulsion motor drive, and using tailless propulsion and control assisted by an onboard stability augmentation system. Drawing on its past experience with flapping wing UAV projects, AeroVironment elected to pursue the project with a small, collocated team of engineers, technicians and experienced model aircraft builders along with a small number of external consultants. From prior experience, the team recognized the great difficulty in optimizing a set of subsystems in theory, then moving directly to the final aircraft integration, especially on such a highly unusual aircraft configuration. As a result, the system would be refined in many evolutionary steps, with frequent prototyping and flight testing.

In 2006, AeroVironment received a Phase 1 contract for the NAV program and was subsequently awarded Phase

¹Principal Researcher, UAS Engineering, 900 Enchanted Way, Member AIAA.

²Senior Research Engineer, UAS Engineering 900 Enchanted Way, Member AIAA.

³Aerospace Engineer, UAS Engineering, 900 Enchanted Way.

⁴Principal Aeromechanical Engineer, UAS Engineering, 900 Enchanted Way.

1B and Phase 2 contracts for continued research and development. By early 2011, the team had demonstrated an 11 minute hover, forward flight to 6.7 m/s, color video transmission with heads-down operation, outdoor flight, and recovery from light gusts. Few remotely piloted ornithopters have demonstrated the ability to sustain hovering flight, with notable examples being the Mentor² from SRI International and the University of Toronto Institute for Aerospace Studies (UTIAS) in 2002, as well as the DelfFly II³ from the Delft University of Technology in 2006. The NAV program was the first hovering ornithopter design effort undertaken at AeroVironment. The two previous flapping wing projects at the company were the Quetzalcoatlus northropi (QN) Replica⁴, and the Microbat⁵, both intended for forward flight only. The QN project created a half-scale replica (5.5 m wingspan) of a giant Pterosaur, on which the flapping wings were responsible for propulsion, lift generation, and control. The Microbat was a smaller scale (23 cm wingspan) ornithopter, which used a conventional tail for control, and flapping wings for lift and propulsion. The Nano Hummingbird differs from other ornithopters in its ability to control attitude in roll, pitch, and yaw during hover through the actuation of the same flapping wings it uses for propulsion, whereas other hovering ornithopters have used large tail surfaces to deflect the wake of the main wings. By performing flight and control with its wings alone, the Nano Hummingbird moves one step closer to nature's flyers, which commonly demonstrate the ability to hover without large tail areas or large tail deflections.

The first part of this paper describes the history of the program, the evolution of the flying prototypes, and highlights the performance and characteristics of the flight vehicle. In the second part, further detailed explanation of the design of the subsystems is provided – wings, flapping mechanism, flight control mechanisms, and onboard avionics – and their own paths of development. The paper concludes with a brief description of the system modeling and analysis environment and then a summary of conclusions and suggestions for future work.

II. Program History and Vehicle Evolution

A. Prototypes

Flying prototypes (see Fig. 2-10) were built as early as possible in each phase of the development program, following the philosophy to 'fly early and fly often'. Table 1 presents the prototypes in chronological order, and summarizes significant features of each. The prototype development goals evolved from investigating inherent instability to propulsion system evaluation to control system refinement. The first flying prototypes were built in order to evaluate the propulsion system performance and potential effectiveness of tail surfaces in hover. Although the overall goal was to develop a tailless aircraft, having a flying prototype with simple tail controls was advantageous to assist in achieving free flight as soon as possible. Tailed prototypes were built with simple "stick-to-surface" radio control (R/C) actuation. The first flying prototype (designated FP1) was built with a relatively large 22.5 cm tip-to-tip wingspan and was capable of forward flight down to very low speeds, but was very difficult to control in stationary hover. This configuration is somewhat similar to the Delft University 'Delfly II' prototype which shows inherent stability near hover using tail surfaces. A second flying prototype, FP2, was built with a 10 cm wingspan, but could not be controlled by a human pilot (even in forward flight). Based on this series of flight tests it was found that to test the smaller scale flapping wings in hover flight, an active, rate based, control system would need to be implemented on the aircraft. Due to the flying difficulties with the FP2 aircraft it was decided to abandon the plan to develop an interim prototype design with large tail surfaces.

Flying prototype 3 (FP3) was the first flying testbed for the flapping wing propulsion system using a custom flight controller and four bidirectional thrusters for control, the wings were not used for control in this case. With rate gyro based controls, FP3 could be hovered for a few seconds which was critical because it showed that the rate gyro signals could be used for flight control even with the high vibration environment of the flapping wing airframe. Prototypes FP5 and FP6 added one axis of wing-based control at a time starting with yaw control, then roll control, and finally pitch control. FP7 was the first prototype to fly with all wing-based control. The Mercury prototype was the first airframe designed as an integrated system, where the airframe was refined and lightened, and achieved a 20 second long hovering flight milestone for Phase 1B. Because Mercury was the first to fulfill a contract milestone

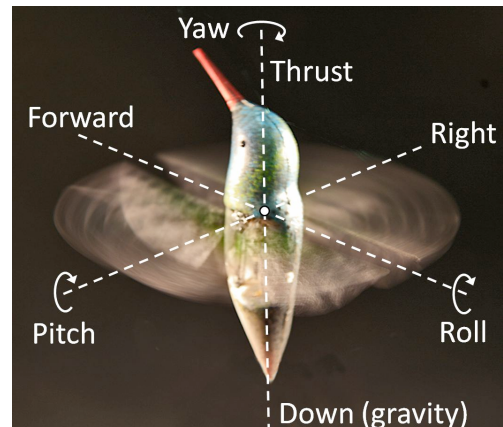


Figure 1. Definitions of Axes. Nano Hummingbird shown with wings flapping in hovering attitude with axes indicated for reference.

flight, it was given a proper name rather than ‘FP8’. After ‘Mercury’ the airframes were all given proper names, and occasionally numbers were added when an airframe had major modifications. The Jupiter series of prototypes tested a second method of wing-based control which was shown to require further refinement. The Saturn prototype was the most lengthy design effort with an advanced miniaturized flapping mechanism and the final miniaturized control mechanism. The final prototype, the Nano Hummingbird was a modification of the Saturn, with the airframe rearranged to fit the biological hummingbird inspired body shell.

Table 1. NAV Program Flight Test Prototypes.

Airframe Name	Date	Contract	Flapping Mechanism	Control System Configuration	Purpose	Outcome
FP1	Nov 2007	Phase 1	Old Microbat Single Lever	Rudder, Elevator Actuator Driven	Test inherent flight stability with tail surfaces, large scale	Successful, near zero flight speed
FP2	Jan 2008	Phase 1	DL2 Narrow Dual Lever	Rudder, Elevator Actuator Driven	Test inherent stability with NAV scale wingspan	Unsuccessful, uncontrollable
FP3	May 2008	Phase 1B	DL2 Narrow Dual Lever	Pitch, Roll Propeller Thrusters	Test gyro operation of stability augmentation system	Unsuccessful due to yaw drift
FP4	Jun 2008	Phase 1B	DL2 Narrow Dual Lever	Pitch, Roll, Yaw Propeller Thrusters	Test gyro operation stabilizing pitch, roll, and now yaw	Success, 14 second controlled flight
FP5	Sept 2008	Phase 1B	DL2 Narrow Dual Lever	Pitch, Roll Thrusters, Yaw Wing Control	Test wing rotation modulation for yaw control	Success with very brief flights
FP6	Oct 2008	Phase 1B	DL9 Wide Dual Lever	Pitch Thruster, Yaw, Roll Wing Control	Test wing rotation modulation for roll and yaw control	Successful flights
FP7	Nov 2008	Phase 1B	DL9 Wide Dual Lever	Pitch, Roll, Yaw Wing Control	Test wing rotation modulation for pitch, roll, yaw together	Successful flights
FP8	Nov 2008	Phase 1B	DL10x Wide Dual Lever	Pitch, Roll, Yaw Wing Control	Test system from FP8 with lightweight flap mechanism	Never flown, flapping mechanism flex problem
Mercury	Jan 2009	Phase 1B	DL10 Wide Dual Lever	Pitch, Roll, Yaw Wing Control	Test all integrated wing controls, stiffened flap mechanism	Successful, 20 second milestone flight
Jupiter 1	Sept 2009	Phase 2	DL10 Wide Dual Lever	Pitch, Roll, Yaw Wing Twist Control	Test all wing twist based controls	Successful, But adverse control cross coupling
Jupiter 4	Mar 2010	Phase 2	DL10 Wide Dual Lever	Pitch, Roll Wing Twist, Yaw Rotation Control	Test pitch, roll wing twist, yaw wing rotation controls	Successful, no adverse controls cross coupling
Gemini	Sept 2010	Phase 2	TD4 String Drive	Pitch, Roll Wing Twist, Yaw Rotation Control	Perform 5 minute hover flight	Successful 6 minute flight, 360° lateral flip
Saturn	Nov 2010	Phase 2	TD5 String Drive	Pitch, Roll Wing Twist, Yaw Rotation Control	Perform 11 minute hover flight	Successful 11 minute milestone flight
Nano Hummingbird	Jan 2011	Phase 2	TD5 String Drive	Pitch, Roll Wing Twist, Yaw Rotation Control	Bird body and video camera integration	Successful flights with video system, body

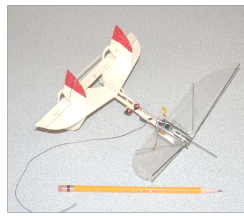


Figure 2. FP1 aircraft.

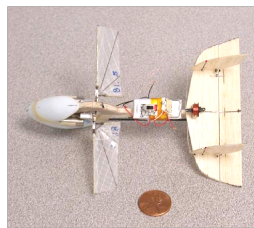


Figure 3. FP2 aircraft.



Figure 4. FP3 aircraft.

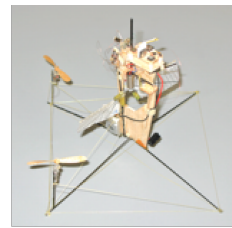


Figure 5. FP5 aircraft.



Figure 6. FP6 aircraft.

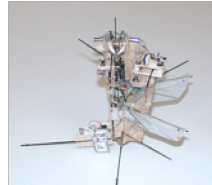


Figure 7. FP7 aircraft.

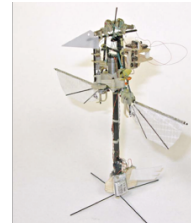


Figure 8. Mercury aircraft.



Figure 9. Saturn aircraft.



Figure 10. Nano Hummingbird aircraft.

B. Development of ‘Nano Hummingbird’ Prototype

The final flying prototype (Fig. 10-12) developed was called the ‘Nano Hummingbird’. The purpose of this final variant was to complete the last Phase 2 DARPA contract milestones which included making the aircraft look like a biological hummingbird, demonstrating heads-down flight using on-board video, maintaining hover in a short duration artificial wind gust, and flying transitions from an outdoor environment to an indoor environment and back again. The prototype successfully demonstrated all of these contract milestones prior to the conclusion of the contract period. Specifications of the Nano Hummingbird are given in Table 2.

The Nano Hummingbird was based on the Saturn prototype, for which significant effort was spent miniaturizing the flapping and control mechanisms while maintaining stiffness and precision. This was a long, challenging process, but led to higher efficiencies and more precise hovering flight. The effort was well spent because the reduction of weight on the Saturn allowed the video system and body panels to be added to the Nano Hummingbird while maintaining acceptable endurance. The wingspan was increased slightly due to pointed tip extensions added to help the cosmetic appearance of the wings. The body shell did not noticeably impact hovering or forward flight performance based on pilot feedback. The mass of the body impacted center of gravity (C.G.) and moments of

inertia, which was taken into account during the integration phase. The battery size was reduced significantly from the Saturn due to space limitations within the bird body shell.

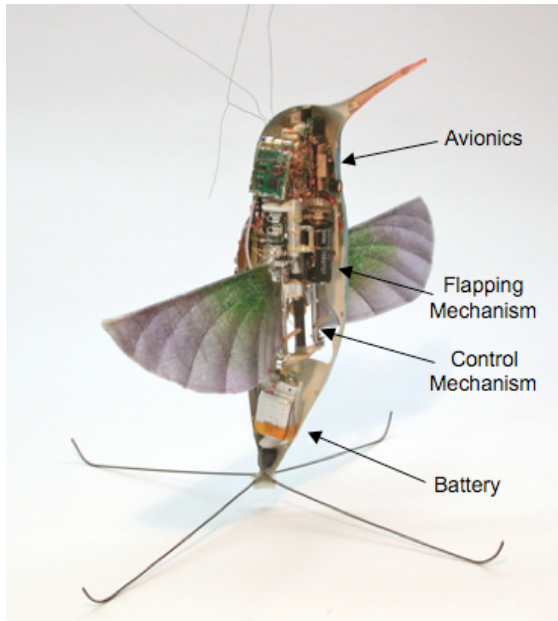


Figure 11. Final Nano Hummingbird prototype
Shown with right body panel removed. Landing gear is optional for flight. Note subsystems fitted into the unusually shaped volume determined by the bird body.

Table 2. Nano Hummingbird Specifications.

Parameter	Value
Total Mass	19.0 g
Flap Rate	30 Hz
Wing Span	16.5 cm
Wing Length	7.4 cm
Speed	Hover - 6.7 m/s (~15mph)
Endurance	4.0 Minutes



Figure 12. Nano Hummingbird and rendering. (a) Early artist's rendering, (b) final aircraft shown in comparison to the rendering.

C. Performance Overview: Long Endurance Configuration

The Saturn prototype was configured for maximum endurance shortly after its initial integration. The goal was to achieve an eight minute minimum hover endurance milestone which was required for the contract. The landing gear was removed, and a battery pack appropriate for the endurance attempt was installed, yielding a relatively high battery mass fraction of 27% (see Fig. 13). Tables 3-5 show the specifications for the Saturn prototype during the 11 minute endurance flight that was ultimately achieved. The parameters are averaged for the entire hover flight endurance. Some parameters varied slightly during the course of the flight. One fundamental design goal was to minimize the power consumption not related to propulsion. For the Saturn that power was kept down to a relatively small 16.5% of the power supplied by the battery.

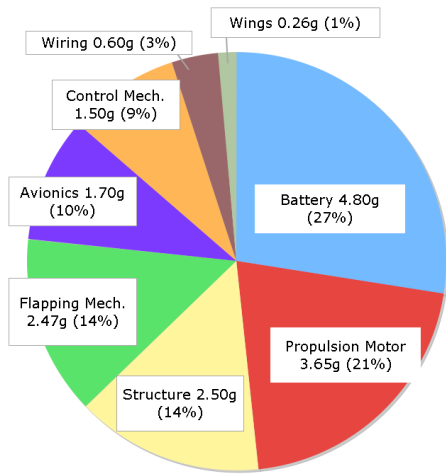


Figure 13. Saturn Prototype Weight Breakdown. Total mass was 17.5g. Weight breakdown for major sub-systems of the 11 minute endurance version of the Saturn prototype.

Table 3. Saturn General Specifications.

Parameter	Value
Total Mass	17.5g
Flap Rate	27.5 Hz
Wing Span	15.8 cm
Wing Length	6.8 cm
Ave. Chord	2.6 cm

Table 4. Saturn Sub-System Efficiencies.

Sub-System	Efficiency
Propulsion Motor	72%
Motor Speed Control	95%
Avionics Power Converter	78%
Gear/Flap/Wing Performance	9.40 g/ W_{shf}

Table 5. Saturn Sub-System Power Utilization.

Sub-System	Power	Percentage
Propulsion Motor System	2.73 W	83.5%
Servo System	0.30 W	9.1%
Avionics	0.24 W	7.4%
Total	3.27 W	100%

D. Program Milestones

The Phase 1 effort concentrated primarily on sub-system research and development. During the Phase 1B and Phase 2 contract periods, several milestone flights were performed (Fig. 15-17) to either test a specific aspect of the system or complete a contract required demonstration. Initial milestone flights were related to hover endurance and hover in place precision. As the prototypes progressed in their capabilities, the milestone flights expanded to more challenging tests such as forward flight, transitions back to hover, gust susceptibility, and heads-down flight via video imagery. One of the more dramatic flight demonstrations was the autonomous 360° lateral flip (Fig. 14) performed by the Gemini prototype in August of 2010, which was a good visual confirmation of the high control authority provided by the control mechanism. All program milestones are shown in Table 6.

Table 6. NAV Program Milestones.

10/2005 – DARPA releases NAV BAA requesting proposals
8/2006 – AeroVironment begins NAV Phase 1 program
6/2008 – First hover flight with flapping wings and augmented stability (FP3)
1/2009 – 20 second hover flight for Phase 1B contract milestone (Mercury)
9/2009 – 2.4 minute hovering flight (Jupiter 1)
3/2010 – First precision hover flight (within 0.45 m radius sphere for 1 minute)
3/2010 – First transition from hover to forward flight and back to hover
3/2010 – First gust susceptibility test
8/2010 – 5.3 minute hovering flight – satisfied Phase 2 endurance milestone
8/2010 – First outdoor flight (Gemini)
8/2010 – First autonomous aerobatic maneuver (360° lateral flip demonstration)
11/2010 – 11 minute hovering flight (Saturn)
1/2011 – First flight w/ hummingbird body & camera (Nano Hummingbird)
1/2011 – First indoor/outdoor transition
1/2011 – First heads-down flight
2/2011 – Met final gust recovery requirement



Figure 14. Aerobic Test.
Gemini prototype performing autonomous 360° lateral flip' initiated by pilot. Image is composite of several frames of video recording.



Figure 15. Saturn endurance test.
The Saturn prototype in steady hover for endurance flight of 11.0 minutes.

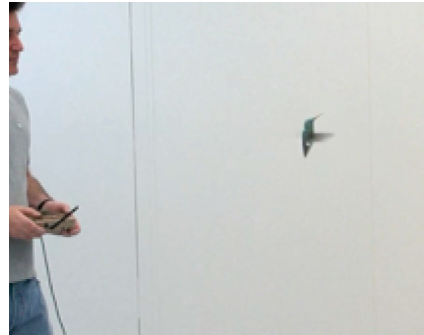


Figure 16. Nano Hummingbird indoors. Flight test without landing gear, aircraft has the most 'biological' appearance in this configuration.



Figure 17. Nano Hummingbird outdoors. Aircraft being flown for the first time outdoors in very light wind conditions. Aircraft performed very well indoors and outdoors based on pilot feedback.

III. Subsystem Development

A. Wing Design

The ultimate goal of the wing design effort on the NAV program was to develop a wing design, which would facilitate both hovering and forward flight capabilities, with a minimum of input power required. Achieving this goal would require the determination of two things: what the time-varying wing geometry should be, and how to build a wing that will achieve the desired shape and motion, in practice.

The use of a flapping wing configuration for the NAV program presented significant challenges in wing design. In the case of flapping wing aircraft, wing design is heavily influenced by the unsteady aspects of flapping – structurally and aerodynamically – as well as planform and airfoil design. The large number of possible degrees of freedom in the kinematics of a flapping wing system make the design problem a complicated one.

Before the wing design process began, the team defined a set of requirements that it felt should guide the design:

- Airfoil camber and wing twist should symmetrically reverse from forestroke to backstroke
- Total wing mass should be low to minimize inertia, and aircraft weight
- Additional structures on wing should be minimized to reduce drag and mass
- Wing should allow modulation of lift and drag for the purpose of control
- Wing must be strong enough to tolerate flapping loads, and rough landing or crash loads
- Wing should be producible in a repeatable, reliable, inexpensive, and timely manner
- Wing should visually look like its biological model in shape and color

Based on the research of earlier ornithopter wing designs and some initial experiments it was thought that the best way to achieve these goals would be through the use of a wing based on a flexible membrane allowed to deform passively. Active control of the wing shape was thought to be infeasible on a reasonable timeline for this project, given the current state of actuator technology, and the resources available.

1. Computational Approach

Past AeroVironment projects such as the Microbat and QN ornithopters provide a possible starting design for the NAV wing, but their flight regime was forward flight, not hover. Thus, a computational approach was employed to design an initial radial planform and twist geometry. The basis of the computational aerodynamics effort are methods developed by Hall^{6,7,8}, and Lebental⁹. In short, this approach uses the minimum induced loss method to determine the optimal circulation distribution. The optimizer finds the best operating point for the airfoil by minimizing the total power required for a fixed thrust. The flapping frequency is then iterated upon to further reduce power consumption. The process is summarized in Fig. 18. The flap stroke amplitude, wing length, and the desired thrust are inputs to this process, as well as constraints on wing chord and lift coefficient. For this application, the wing length and desired thrust were dictated by the DARPA requirements, flap stroke amplitude was chosen to be 180°, and XFOIL¹⁰ was used to generate the lift curves and drag polars (NACA 0009). Lacking any mechanical requirements at the time of design, a maximum chord limit was placed on the process that kept the appearance of the wing aesthetically similar to a natural hummingbird.

The use of computational aerodynamic design tools provided a starting point for the wing design process, but alone did not account for two major factors. First, losses incurred by the flapping mechanism were neglected, which as will be shown later turn out to be a significant portion of the propulsion system power usage and increase

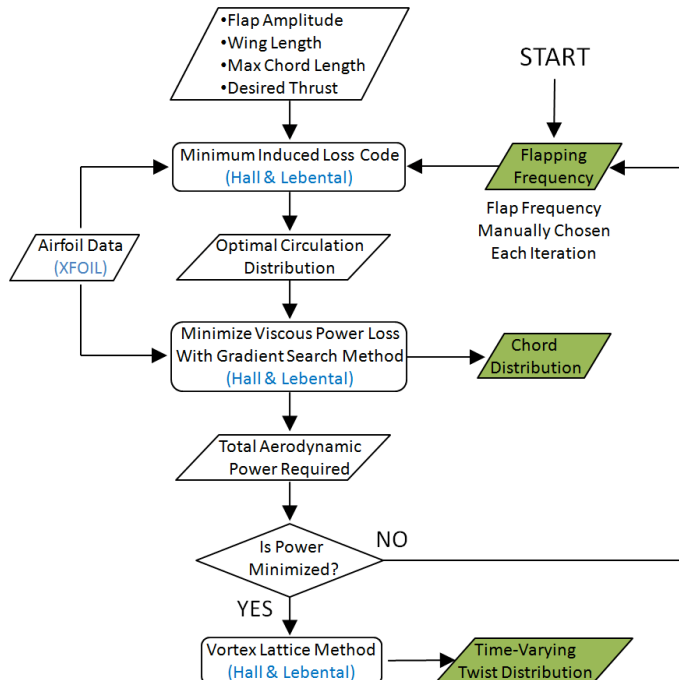


Figure 18. Flow diagram of computational wing design

dramatically with both flapping frequency and wing angular inertia. Later in the program, these effects were taken into account in the system analysis environment, but only after building a large database of wing performance through experimentation. The second missing factor was a means of guiding the structural design of the wing to ensure that the desired twist distribution and airfoil camber are achieved when the wing is flapped in practice. The membrane based structure which inherently allowed airfoil symmetry and later a method for control was very difficult to predict in a dynamic environment. These factors to wing design were most readily addressed by moving to an experimental based wing design approach.

2. Experimental Approach

Experimental techniques were used heavily in the wing development process. Experiments were used to evaluate the wing designs produced by the computational tools, as well as those based on intuition and creative problem solving in a heuristic manner.

Quantitative analysis of wings was based around the metric of thrust per motor shaft power as mechanism power consumption is not readily separable from the aerodynamic power (see section on *flapping mechanism performance*). Shaft power was converted from motor input voltage and current using a well tested model of the drive motor. The primary tool for thrust measurement was a thrust plate mounted on a gram scale and positioned in the wake of the wing to be tested. Using this approach, the gram scale should measure a force equal to the thrust created by the wing. This is a convenient way to measure a time-averaged value of the thrust, and separate the measurement of aerodynamic forces from inertial forces. This approach was compared against tests in which a proof mass was lifted directly. Tests with multiple wing sets of varying design showed the thrust plate method to consistently overestimate thrust by approximately 10%. All thrust data presented here should be assumed to include the roughly 10% error known to be associated with the thrust plate measurements.

Over the course of the program, thrust per unit motor shaft power was used as the primary metric of wing efficiency. Each wing design was tested and compared to a baseline wing. Because the thrust to power ratio is heavily influenced by the wing length (see Fig. 19), wing design changes needed to be compared to a baseline wing of comparable length (in contrast to the *figure of merit*, used in helicopter performance).

Qualitative aspects of wing design were numerous and included durability, manufacturing repeatability, camber reversal behavior (aside from efficiency implications, it also affected controllability), and acoustic signature. A host of tools were employed including stroboscope and high speed video which allowed detailed visual inspection of wings at any moment in the flap cycle.

Early in the program, wing development focused mainly on learning to control wing shape - camber and twist - passively during flapping. Wing behavior at the stroke reversals was also found to be important, but particularly difficult to control. As the wing slows down at the reversal, the aerodynamic forces decrease significantly, allowing inertial forces to become the dominant factor in wing deformation. A combination of qualitative visual evaluation and quantitative performance measurements showed that performance degraded as the camber reversal period increased. As a result, one important goal in the heuristic wing design process was to implement ideas thought to improve the expediency of the camber reversal process.

Build repeatability and durability were also important criteria in the wing design. Under the harsh flapping conditions, wings tended to tear and fray which caused flight failures, reduced performance with time, as well as considerable maintenance effort. Manufacturing repeatability was equally important because an aircraft with asymmetry in left to right wing characteristics can result in an uncontrollable vehicle. This was especially important because wings were hand crafted. Many wing design features were added to improve durability, and wing build fixtures were developed over the course of the program to improve repeatability.

One feature common to nearly all wing designs was the use of a basic frame consisting of a spanwise main spar and a chordwise root spar, both made of carbon fiber. This type of frame in combination with diagonal battens on the wing membrane is the same type of structure used on the Microbat, and most commonly on free flight model

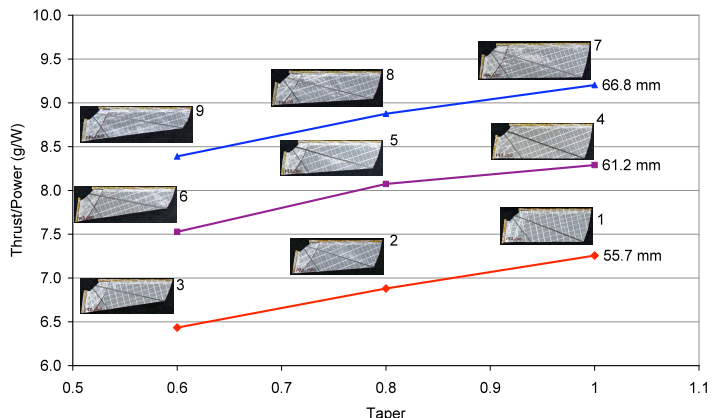


Figure 19. Thrust per unit motor output shaft power vs. taper ratio and aspect ratio. Lines connect wings of constant length. All thrust measurements made with thrust plate.

ornithopters. Most notably, this batten layout provides reliable camber reversal, high efficiency camber and twist distribution, and an ease to manufacturing. A representative wing membrane design is shown in Fig. 20 without the carbon frame.

Many different wing membrane materials were attached to such frames for testing. Membrane materials ranged from completely solid to highly porous, from easily stretched to highly reinforced with minimal stretch, and from very loose to relatively stiff. Rigid wings with symmetric airfoils were also built and tested in arrangements where they were allowed to rotate about the main spar for stroke reversal. Also critical to the dynamic behavior of the wing is the design of the main spars, as well as reinforcements placed on the wing membrane. Spar flexibility was varied for testing through either selection of carbon fiber rods of different diameter, or the use of custom equipment to taper the carbon rods. Structural reinforcement on the wing membrane was tested in many forms, including the conventional batten or multiple battens, adding multiple layers of the membrane material or adhesive tape in specific locations, and the addition of fibers or filaments. A sample of the approximately 300 wings designed and tested over the period of the NAV program are shown in Fig. 21.

3. Acoustics

In general, flapping wing vehicles are prone to generating high noise levels because the oscillatory motion tends to induce vibrations throughout the wing and vehicle. Hummingbirds alleviate this effect through the soft structured wings, as well as a low disc loading and very light structural weight. Other natural fliers, such as large Asian beetles have higher disc loading and membrane type wings which result in much louder signatures. The disc loading and wing structure of the Nano Hummingbird leans more towards that of the large beetles than the hummingbird.

In a parallel development effort, the acoustic signature of the flapping mechanism and wings were studied through the use of high speed audio and video equipment. The goal was to identify the most significant sources of noise.

The high speed video and audio recording were performed simultaneously on wings producing nominal thrust. The recordings were synchronized, and later combined into a video which displayed the acoustic signature in graphical form along with the video of the wing itself. A snapshot of synchronized video and audio data is seen in Fig. 22. The upper video shows the wing throughout the flap cycle, with this particular frame captured during the airfoil reversal. The lower left graph shows the time history of the A-weighted sound pressure level (SPL), with the red line indicating the time of the current video frame. The lower right graph shows the spectral distribution of noise at the given time.

The results of the video tests immediately showed that the majority of the noise was produced during the stroke reversal portion of the flap cycle. The large acceleration during this period caused the wing membrane to pop through from the fore-stroke configuration to the aft-stroke configuration in an unstructured and violent manner. This is similar to how the sail ‘pops’ on a sailboat as the sail rotates during a ‘tack’.



Figure 20. Nominal style wing design used throughout the NAV program.



Figure 21. Some examples of wing designs tested during the NAV program.



Figure 22: A snap shot of a wing flapping on a bench test flapping mechanism, with synchronized acoustic signature.

B. Flapping Mechanism Design

1. Four-bar Linkage-Based Flapping Mechanism

For the flapping mechanism sub-system, the initial plan was to build on what was known to work from the previous Microbat MAV ornithopter flapping wing prototype which was an efficient, low amplitude design. That aircraft used a simple planar four-bar linkage of the crank-rocker type. Several years were spent on that project learning how to design and fabricate lightweight, high power handling flapping mechanisms using gears, cranks, bushings and levers. The baseline approach on the NAV project was to use what was known from Microbat as far as mechanism weight, powers, and efficiencies to help generate a starting point for the NAV power and weight budgets. This worked out well, and the flapping mechanisms (including the gear train) had acceptable performance, even from the start. The philosophy of continuous evolution, improvement through testing, analysis, and re-design, had allowed a progression towards a small, lightweight and compact mechanism.

For NAV, the goals were to obtain a large stroke flapping amplitude using a DC electric motor with on-board battery. The first new design utilized was a dual, series, four-bar linkage. Early designs were based on the Microbat style of crank-rocker linkage, with a second four-bar added to allow higher flap amplitudes ($>180^\circ$) as shown in Fig. 23. Ten major iterations of this design were fabricated (DL1- DL10, for “dual-lever” 1 through 10). The DL1 unit (Fig. 24) was the main bench test mechanism, built massive and strong for durability. The DL2-DL7 mechanisms (Fig. 25) were a series of similar half scale versions of DL1, lightened for use in initial flying prototypes. For the DL8 and DL9 mechanisms, the flap axis separation was doubled to allow for the flight controls mechanism to be mounted between the wings. For the DL10 design, major aluminum components were replaced with polyetheretherketone (PEEK) plastic parts for a significant weight reduction (Fig. 26).

The dual lever type mechanism was used on prototypes FP2 through Jupiter 4. This was a very successful mechanism overall, but had problems with mechanical wear. The wing mounts, links, and pushrods would wear and occasionally fracture and fail over time. These repairs were very time consuming, so a more durable, but lightweight design was needed. Radial play in the bushings caused spikes in the wing accelerations which caused reduced wing efficiency based on comparative tests between before and after replacing the bushings. Weight, durability and dynamic performance problems with the dual lever mechanisms led to the need for a new approach, which became the string-based flapping mechanism.

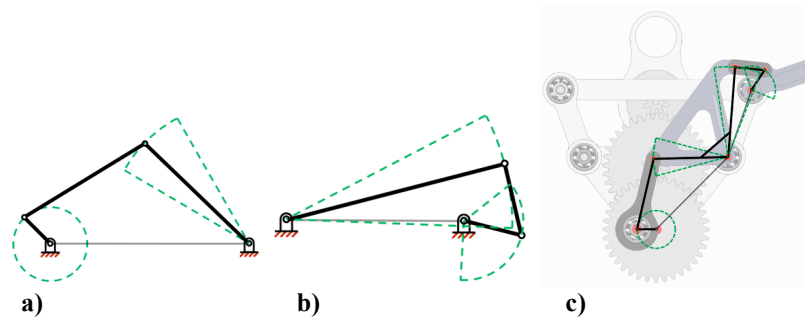


Figure 23. Dual Series Four-bar Linkage Design. (a) Basic ‘crank rocker four-bar linkage’ converting rotary to oscillating motion. (b) ‘Double rocker four-bar linkage’. (c) Both of those systems are combined in series to produce the dual lever flapping mechanism shown overlaid onto the DL10 design. The output of the crank rocker is rigidly attached to the input of the double rocker.



Figure 24. 'DL1' Dual Lever Flapping Mechanism. 13 grams, primarily fabricated from 7075 Aluminum, used for bench testing only.



Figure 25. 'DL2' First Miniature Dual Lever Flapping Mechanism. 2.5 grams, used on the first hovering free flying prototypes.



Figure 26. 'DL10' Dual Lever Flapping Mechanism. 2.8 grams, primarily fabricated from PEEK plastic.

2. String-Based Flapping Mechanism

To address the issues associated with the dual lever mechanisms, a solution was sought that would reduce the number of bearing surfaces, the amount of oscillating mass, and the overall mass. The string drive addresses these issues by using a tension-based system in contrast to the four-bar linkage-based system which operated in both compression and tension.

The mechanism uses a continuously rotating crankshaft driven by an electric motor in the same manner as the dual lever based mechanisms. The pin on the crankshaft has two strings attached, each one connected to two pulleys which are mounted on the wing hinge flapping axes (Fig. 27, red and blue strings). As the crankshaft turns, the pulleys oscillate. Two additional strings (Fig. 27, green and black strings) connecting the pulleys keep the two pulleys (and wings) matched in phase, and also maintain tension on the drive strings. The resulting motion is shown in Fig. 28.

The first string drive prototypes were developed in parallel with the latter variants of the dual lever designs because it was known that the dual lever design had problematic limitations, but actual working flapping mechanisms were needed in the interim to continue the controls and airframe development. The first string drives were very large in size, and were not initially considered viable for flight use.

After further iterations a string drive concept of reduced size was conceived and fabricated for flapping a single wing and test data showed comparable system efficiency to the dual lever mechanisms. The design was then expanded to flap two wings simultaneously, maintaining good phase relationship between the two wings, which was a highly desirable characteristic to minimize vibration and maximize thrust.

The final string mechanism, shown in Fig. 29 was the design used initially in the Saturn prototype. It was designed to be lightweight, efficient, durable, easy to maintain, easy to fabricate, integrated into the control system, and a main structural element of the airframe. Like all of the machined parts, it was fabricated in-house at AeroVironment. The main structure was cut from 7075 Aluminum for the main components, and other components were steel and titanium. Ball bearings were used for their long operating lifetime. A system was developed to allow the adjustment of each of the string lengths by means of small rotating pins, so each string

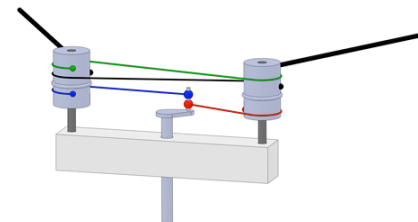


Figure 27. String based large amplitude flapping mechanism design. Central crank rotates, pulls on strings and drives the two pulleys in oscillating motion.

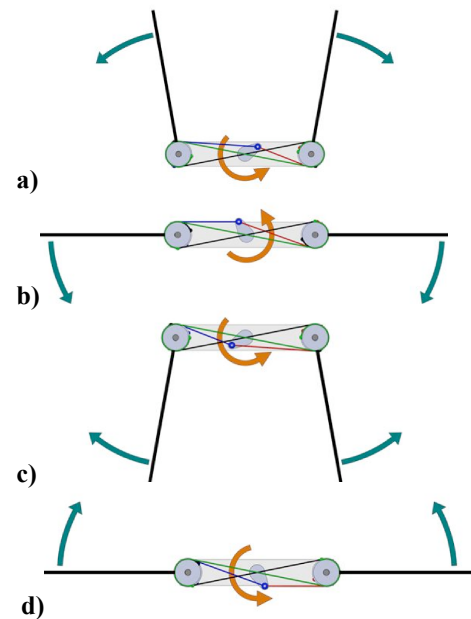


Figure 28. String based flapping mechanism geometry. Figures (a) and (b) are forestroke motions, (c) and (d) are backstroke motions.

could be adjusted similar to tuning a string on a violin. Multiple strands of strings were used in parallel to allow high flexibility but also maintain a very high tensile strength.

A comparison was made between the flap stroke profile of the string-based system and the linkage-based system. Four small and lightweight LED lights were installed on each flapping mechanism, two at the leading edge spar tips, and two at the centers of the wing hinges. High speed video captured the dots of light from the LEDs, and the video was processed to determine the wing angular position, speed, and acceleration for several wing beats. The resulting data allowed comparison of actual hardware to the computer models for the string-based, and also the linkage-based systems giving quantitative comparisons of different mechanism designs and their simulations.

In Fig. 30, the data for the DL10 with a pair of baseline wings is shown. Note left-right asymmetry in acceleration which correlates to asymmetric forces, and thus vibration on the airframe. This observation helped confirm the need to evolve the flapping mechanism to a more symmetric design. Flap stroke data for the string-based system is shown in Fig. 31. Note that for the string-based system, the flap angle profile is closer to a sinusoid, and also the amplitude of the tip accelerations is considerably lower than the linkage-based system.

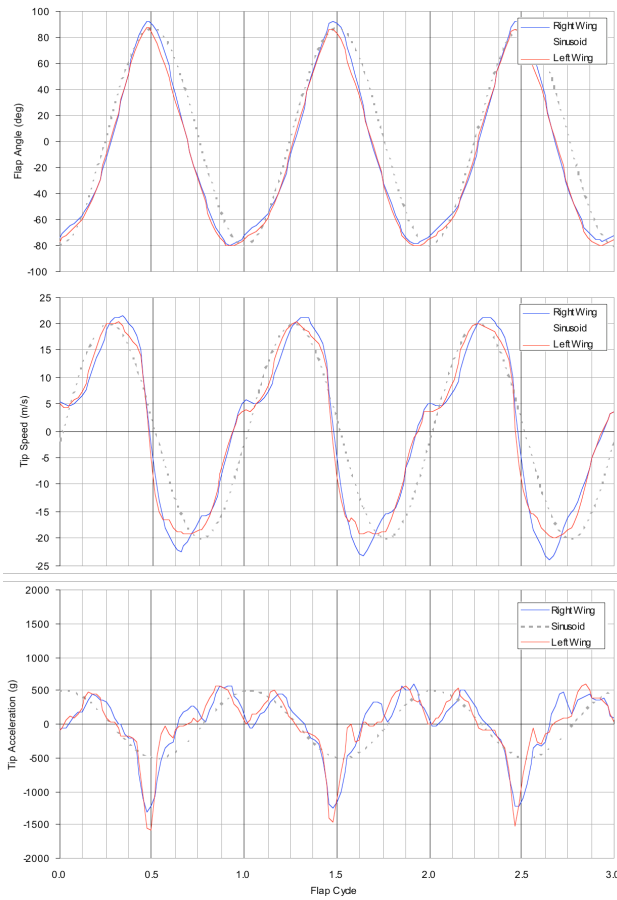


Figure 30. Linkage-Based Stroke Profile.
DL10 Mechanism, 40 Hz Flapping 180°.

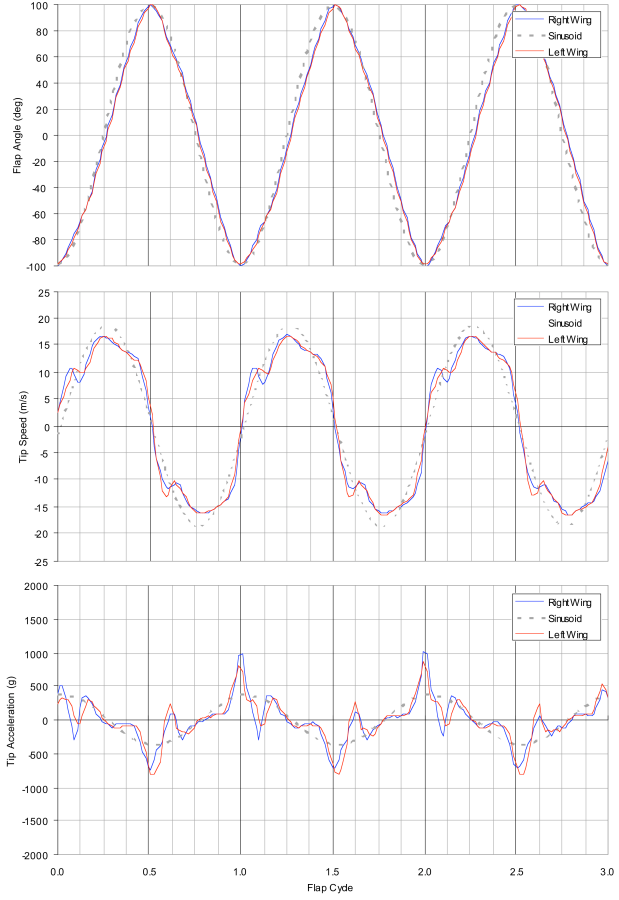


Figure 31. String-Based Stroke Profile.
33 Hz Flapping 200°. Note in this test, and DL10 test, the net static thrust was equal.

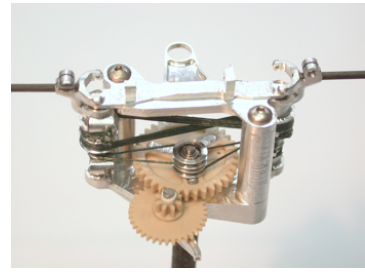


Figure 29. Final string based large amplitude flapping mechanism. Aluminum frame with PEEK gears used in Saturn and Nano Hummingbird aircraft.

3. Flapping Mechanism Performance

The problem of measuring the mechanical power delivered to the wing is a complicated one, even when the electrical power supplied to the drive motor is well known. During all wing tests, a well-characterized motor was used to power the DL1 mechanism. Based on past experimental data as well as testing on a custom micro-dynamometer, the efficiency, or ratio of output shaft power to input electrical power of this drive motor could be determined with a high degree of confidence at any operating condition. However, the efficiency of the flapping mechanism and geartrain, which converts the motor shaft output to wing motion was not well-known.

One approach suggested for measuring the power absorbed by the mechanism was to run the system in air, then run the system at the same flap frequency in a vacuum where the aerodynamic power required to generate the desired thrust would be eliminated, and compare the power required. While this method eliminates the power consumed overcoming aerodynamic drag, which is considered aerodynamic power, the lift and drag forces also induce friction within the mechanism, which will not be experienced in the vacuum. Also, the wing membrane will not behave the same as in air, where the air fills the sail and dampens the motion at stroke reversal, thus altering the inertial forces induced by flapping.

A set of vacuum chamber experiments were run as a means of estimating power loss in the flapping mechanism, and its relationship to flapping frequency and wing angular inertia about the flap axis. Figure 32 shows the vacuum chamber setup with the flapping mechanism installed. Wings of varying inertia were flapped in the chamber at varying frequencies. Motor electrical input voltage and current, as well as flapping frequency were measured to allow for the determination of motor shaft output power at each test condition from independent dynamometer tests. Results of the vacuum chamber tests indicated that power absorbed in the flapping mechanism increases rapidly with flapping frequency and wing angular inertia, as shown in Fig. 33.

This strong relationship between mechanism power consumption and flapping frequency revealed a major issue with the computational wing design approach. Because these tools did not account for power loss in the mechanism, wing designs were not penalized for operating at very high frequencies, which the optimizer tended to favor. Although these designs may have approached the highest aerodynamic efficiency, they did not result in the highest propulsion system efficiency. Following the vacuum chamber experiments, test wings of similar style and identical span, but with larger wing area were built with the intent of developing the desired thrust at a lower flapping frequency. Preliminary tests of these wings showed reduced motor shaft power required to develop hover thrust, indicating an improvement in efficiency of the wing and flapping mechanism propulsion system.

Because of the difficulty in isolating flapping mechanism losses, it was decided that wing designs should be compared in terms of their performance as part of the propulsion system, rather than purely on aerodynamic performance. Therefore, the primary metric for evaluating wing designs became motor shaft output power required to generate a given average thrust. Although the use of this metric complicates analysis of the wing from an aerodynamics standpoint, it is actually relevant because the wings will never be decoupled from the flapping mechanism on the real vehicle.

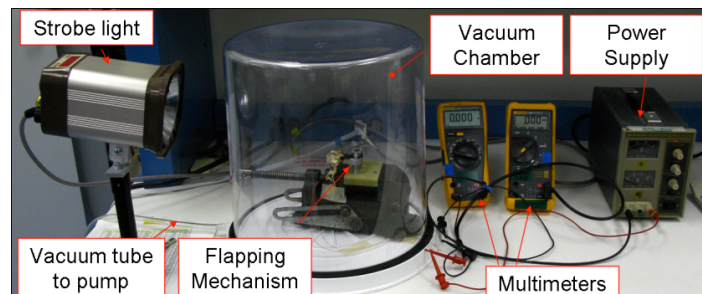


Figure 32. Vacuum chamber setup for flapping mechanism power loss testing.

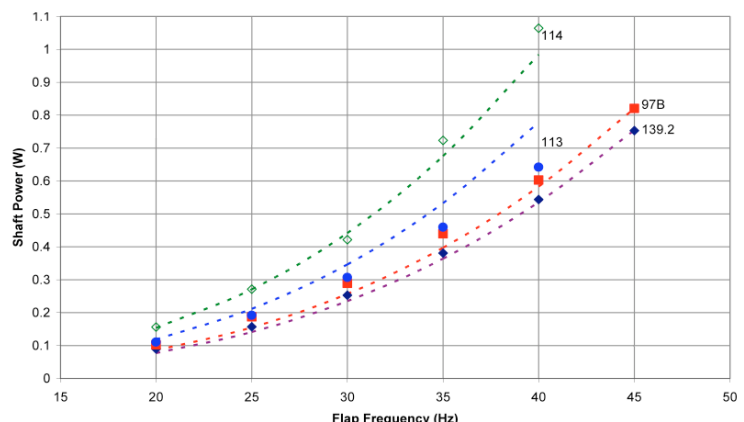


Figure 33. Shaft power measurements in vacuum for wings of varying angular inertia at varying flap frequency.

C. Control Mechanism Design

1. Tailless Control Approach

For basic aircraft flight control, the goal was to generate controlling moments in the roll, pitch, and yaw axes using only the flapping wings. In roll and pitch, the control system for the flapping wing vehicle operates similarly to a helicopter in that lift production is modulated depending on where the lifting surface is relative to the body. For example, a positive roll moment is created by

increasing lift production on the left side and reducing lift on the right side (Fig. 34). Similarly, a positive pitch moment is created by increasing lift on the fore end of the flap stroke and reducing lift on the aft end (Fig. 35). Yaw moments are created through two possible mechanisms: a positive yaw moment is created by 1) increasing the average drag on a wing as it moves in the counter-clockwise direction, or 2) tilting the right stroke plane back and the left stroke plane forward.

To achieve these modulations, various approaches were considered, including variable flap amplitude, variable flap stroke centering, variable wing twist/pitch, and flap plane tilting (thrust vectoring). The project focus was placed on the development of two methods: wing rotation modulation and wing twist modulation. These methods can be implemented in a way much like that of the helicopter swashplate in that control can be input through the actuation of a non-rotating/non-oscillating element which is transferred to the wings as a cyclic actuation of the lifting surface. This approach seemed familiar and less complicated than the other methods which would likely increase the complexity of an already complex flapping mechanism. The development of control mechanisms using pure wing rotation, pure wing twisting, and a hybrid system which was used in the final Nano Hummingbird design are described in the following sections.

2. Wing Rotation Modulation

The first approach to wing-based flight control used wing rotation modulation. In this approach, wings are allowed to rotate passively about the leading edge. Aerodynamic force tends to push the wing to align with the flow, similar to the boom swinging into position on a sailboat. Two adjustable ‘stops’ limit how far each wing can rotate under aerodynamic and inertial loads, setting the nominal wing rotation angle for each half-stroke, as shown in Fig.

36 and Fig. 37. Angle of attack is increased or decreased by changing the wing rotation angle, which results in changes in both lift and drag. Modulation of lift and drag in this way can be used to affect control moments as described in the *Tailless Control Approach* section, using differential drag for yaw control.

Different types of wing

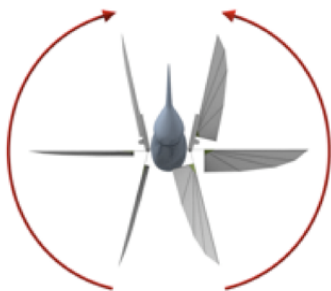


Figure 34. Roll control (top view). The left wing has a higher angle of attack than the right, and the vehicle rolls to the right.

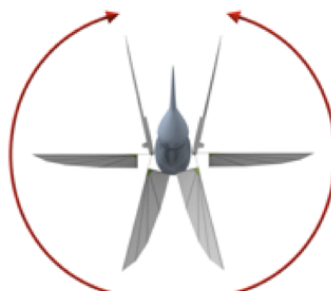


Figure 35. Pitch control (top view). Both wings increase angle of attack during the fore portion of the stroke, and the vehicle pitches up.



Figure 36. Lift modulation using wing rotation stop modulation. Flapping in the horizontal plane. (a) wing is at high angle of attack yielding high lift, (b) low angle and low lift.

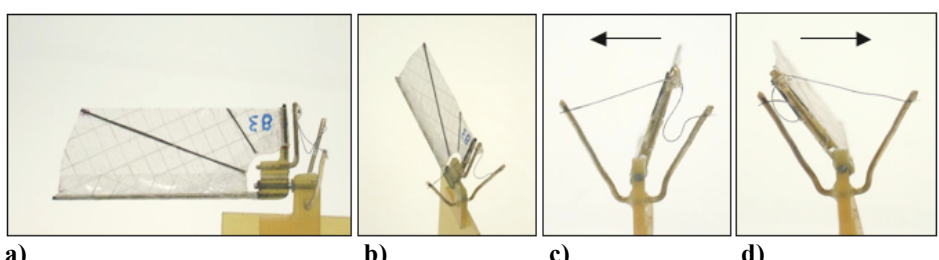


Figure 37. Conceptual model of string based wing rotation modulation. Lift and drag modulation using variable wing rotation. Wing rotation stops are strings of different lengths, yielding asymmetric lift and drag on the forestroke vs. downstroke.

rotation stop concepts were tested including rigid levers, strings, and a combination of strings and levers. The practical challenge was transmitting the control forces from the fixed body system where the actuators would normally be located to the moving wing systems without loss of force or loss of precision. This wing rotation stop modulation system was used for the first successful hovering flights with wing-based control. Systems of strings were used to transfer the controls from the body to the moving wings taking advantage of the flexibility of the strings. This system had significant acoustic noise, control precision problems, and sub-optimal wing efficiency performance but did allow minimally acceptable control.

3. Twist Modulation

A second approach to aircraft flight control using only the wings was developed and ended up being used in the Phase 2 aircraft. The system generated control moments by varying the amount of twist in the wing membrane. This design change was also performance driven, as it was known that highly twisted wings were more efficient aerodynamically than low twist wings. The previous wing rotation control method was not very effective at modulating lift with highly twisted wings. In addition, there were difficulties with the practical implementation of the mechanical systems necessary for the wing rotation design.

Experiments showed that lift and drag could be modulated by changing wing twist distribution, from a slightly twisted, to a highly twisted shape. The flexible wing membrane is allowed to deform passively, but the twist distribution can be influenced by tightening or loosening the membrane, similar to a sailboat sail. The wing membrane is allowed to rotate freely about the leading edge, and tightened or loosened by changing the angle of the root spar with respect to the leading edge, as shown in Fig. 38. Modulating the root spar positions laterally affects membrane slack primarily near the midstroke, which can be used for roll control. Moving the root spars forward and aft affects membrane slack primarily near the stroke reversals which can be used for pitch control. Combining root spar movements in different ways can result in moments on the vehicle in all three of the desired axes (roll, pitch, yaw), as shown in Fig. 39 and Fig. 40. Experiments showed small changes to the wing twist generated relatively large moments as compared to the wing rotation modulation system.

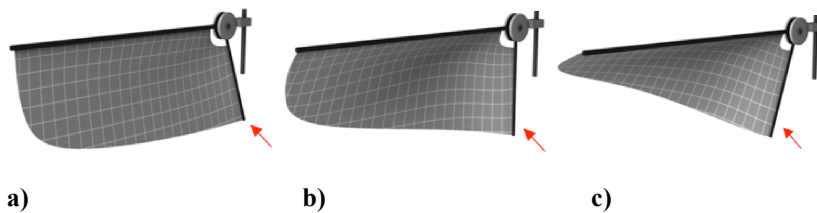


Figure 38. Concept Of Variable Wing Twist Modulation. Root spar (indicated by red arrow) rotates away from the wing membrane to increase lift (a) and towards wing membrane to reduce lift (c).

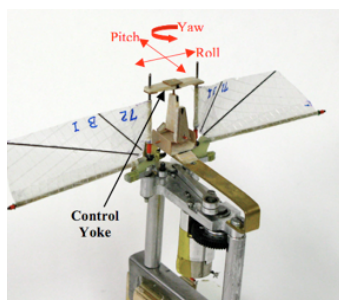


Figure 39. Design mockup of the variable wing twist control system. Arrows indicate the directions of movement of the end of the root spars to generate the desired

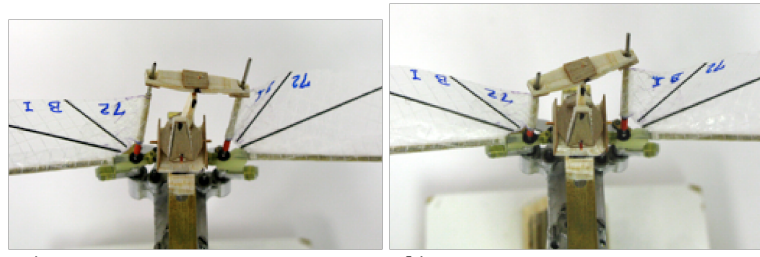


Figure 40. Mockup of mechanism to modulate wing twist. (a) Roll command with low twist at left, high twist on right wing. (b) Yaw input where right and left wings are modulated in opposite directions between forestroke and backstroke.

4. Combined Wing Twist and Rotation Modulation

The wing twist modulation control system had excellent single axis controllability, was not a detriment to propulsive efficiency, was quieter than the wing rotation system, and was an elegant design solution. The system was implemented in the Jupiter series of aircraft which had many successful flights, but would occasionally diverge in roll before the pilot or control system could compensate. This phenomenon was investigated on the bench by attaching the flight vehicle to a six degree of freedom (6-dof) torque and force transducer (see Fig. 41). Test measurements quantified the problem, which could readily be seen as an undesired roll moment appearing with combined pitch and yaw inputs (see Fig. 42). The magnitude of the undesired roll moment was too large to be compensated by a roll input.

To correct the control cross coupling effects, either the pitch or yaw control system would have to be changed. Yaw control by wing rotation had previously shown high authority and based on experience it would be easier to implement than pitch by wing rotation or some other pitch control system. A hybrid system was prototyped using wing rotation modulation for yaw control and wing twist modulation for roll and pitch control. The CAD model and fully assembled, functional hybrid designs are shown in Fig. 43 and 44 respectively.

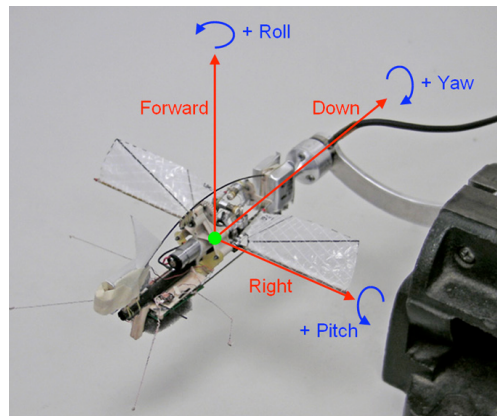


Figure 41. Bench test setup for measurement of control moments. A 6 degree of freedom transducer seen at base of aircraft reported output moments in all axes given any combination of control inputs.

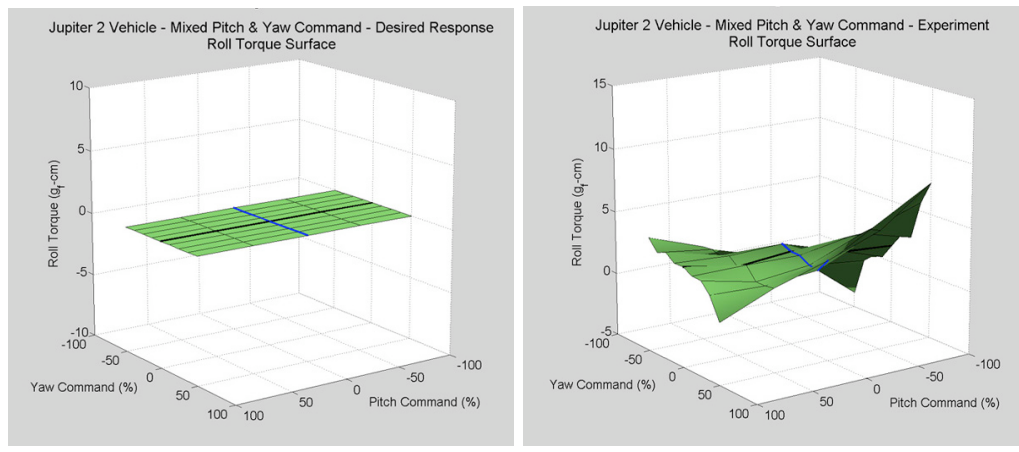


Figure 42. Pitch and yaw control test. Roll channel moment desired (a) and measured (b) as a function of pitch and yaw inputs with a pure twist modulation control system. Note that large pitch and yaw inputs result in an undesired roll moment.

Prior to implementing the hybrid control system on a flight vehicle, the control characteristics were measured. The results, which are displayed in Fig. 45, showed improved control characteristics with respect to cross coupling, and specifically the pitch/yaw to roll coupling. Additionally, single axis control authority was preserved and combined axis control authority was acceptable. After integration of the flight vehicle around the new hybrid control system and tension drive flapping mechanism, it was found that acceptable control authority was available in all axes throughout all types of flying maneuvers including some aerobatics. This hybrid control system became the final design to be implemented in the NAV program.

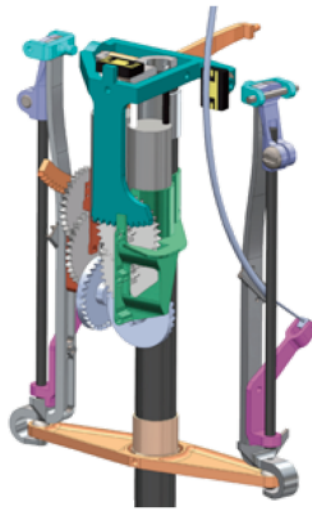


Figure 43. CAD model of hybrid control system mechanism. The central post tilts in two dimensions for pitch and roll control. The purple arms rotate differentially for yaw control. The two black vertical rods are the root spars.



Figure 44. Actual control mechanism. System installed on Saturn and Nano Hummingbird. Aluminum, plastic, and carbon structure.

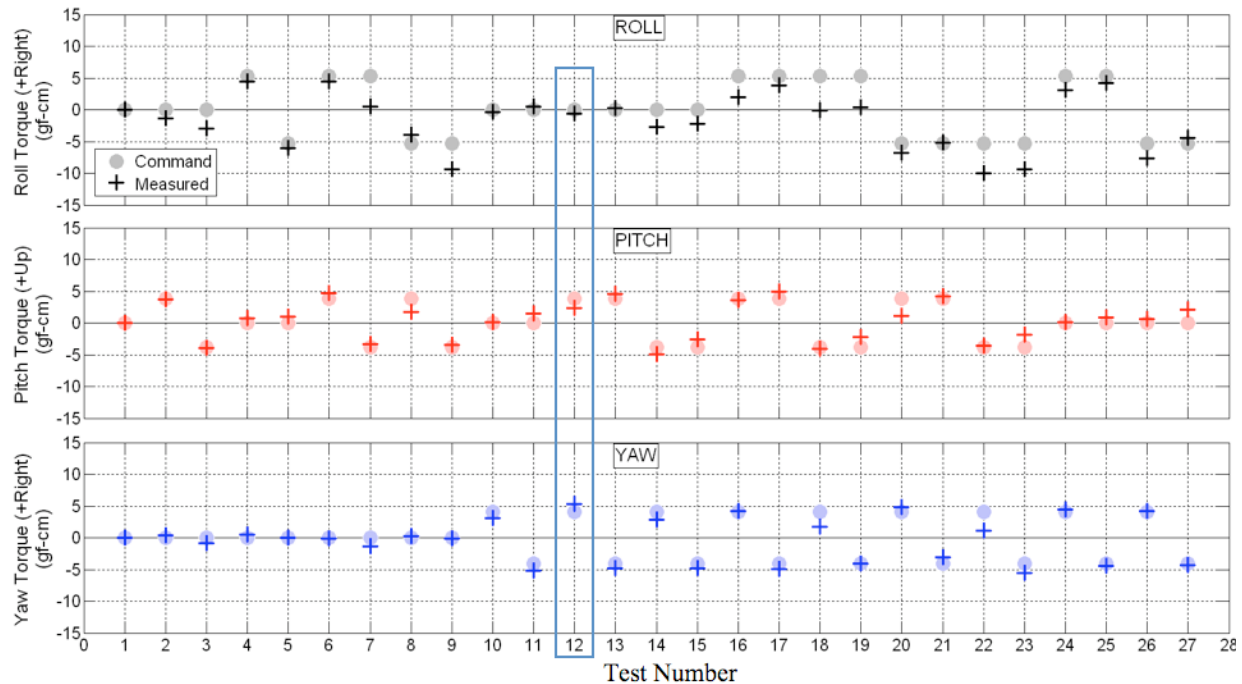


Figure 45. Hybrid control mechanism test results. Each numbered test (*x*-axis) was a unique combination of roll, pitch, and yaw inputs (given here as moment commands), which resulted in the measured moments .

D. Avionics

The DARPA requirements for the NAV program did not include fully autonomous operation of the aircraft. From the beginning of the program, the AeroVironment NAV was designed with the intent of being flown either "heads-up", where the pilot flies the aircraft by looking at it directly, or "heads-down" where the pilot flies the aircraft through onboard video, downlinked in real-time. Because inherent stability was not designed into the aircraft, the avionics would also provide stability augmentation to assist the pilot in controlling the vehicle.

All revisions of the NAV avionics utilized commercial-off-the-shelf (COTS) components on custom-designed circuit boards. The core of the avionics suite contains a single microcontroller unit (MCU) to manage all electrical systems, microelectromechanical systems (MEMS) rate gyroscopes (3 axes) for stability augmentation, a receiver for obtaining commands from the pilot, driver circuits to operate the propulsion motor for wing flapping and actuators for control, and components for DC power conversion. This collection of core components is referred to as the flight controller (FC).

Two major revisions of the FC were developed, each of which was first prototyped without a printed circuit board (PCB). As shown in Fig. 46, components were built up in "dead bug" style, and wired together on a wooden substrate. This approach provided flexibility for swapping candidate components for performance evaluation on the aircraft, and eliminated the time and financial costs of designing and fabricating multiple PCB revisions.

Throughout Phase 1 and Phase 1b, wooden substrate FCs were used to fly the prototype vehicles. In Phase 2 of the program, the FC underwent major changes, including upgrades of the MCU and gyroscopes, replacement of the discrete driver circuits with DC motor driver integrated circuits, and the addition of a flash memory chip for onboard data logging. PCBs were designed and fabricated for the FC in Phase 2, and by the end of the program, three revisions of the FC PCB had been fabricated. The final revision of the FC is shown in Fig. 47. Fully assembled, this circuit board has a mass of 0.65 g, and was designed to fit in a specific location underneath the hummingbird-shaped body fairing of the Saturn prototype.

The software running on the MCU was developed in-house, and is responsible for stabilizing the vehicle, interpreting and executing control commands from the pilot, logging data, and general supervisory tasks. Closed-loop control is performed by the MCU on yaw, pitch and roll rates, positions of the yaw, pitch and roll servos, and the wing flapping frequency. Using the ground station, the pilot commands flapping frequency, yaw rate, pitch rate, and roll rate.

The use of a flapping-wing configuration with only two wings leads to a vibration environment onboard the NAV, which differs from that normally found on fixed-wing or rotary wing aircraft. The use of only two flapping wings introduces some unavoidable issues. As the wings alternate between creating lift in front of, and then behind the C.G., the vehicle is subject to a continuous oscillation in the pitch axis. A similar issue is the inertial forces resulting from the repeated acceleration and deceleration of the wing masses during flapping, which is unbalanced in the forward and aft directions. Experimental evaluation of multiple Coriolis vibratory gyroscopes from different manufacturers revealed that despite nearly identical specifications on their datasheets, some gyroscopes behaved much differently in the NAV vibration environment than others. Fig. 48 compares the output of parts from two manufacturers, having identical full-scale measurement ranges, mounted identically on the vehicle as the wings flapped at a frequency of 40 Hz. It can be seen that one gyroscope saturates, while the other does not. These data illustrate the importance of choosing gyroscopes that are well-suited to the vibration environment of a flapping wing vehicle.

Early in Phase 1, it was understood that the NAV would be sufficiently small, light, and unstable such that if left uncontrolled, the aircraft would diverge rapidly. For this reason, high speed control actuators would be required. Due to the overall challenge of weight and power, the actuators would also need to be lightweight and consume minimal power. Shape memory alloy and piezo based actuators were investigated, but practical solutions using these technologies did not meet the baseline requirements for speed, weight, power, travel, and force outputs. The approach taken was to use conventionally designed servo actuators using the smallest available DC brush electric motors, and combine those

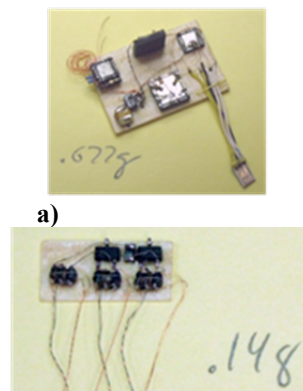


Figure 46. Flight controller for Phase 1 prototype aircraft. Includes (a) MCU, COTS receiver, gyroscopes, and (b) motor driver circuits.

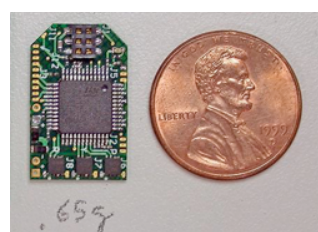


Figure 47. Final revision of flight controller.

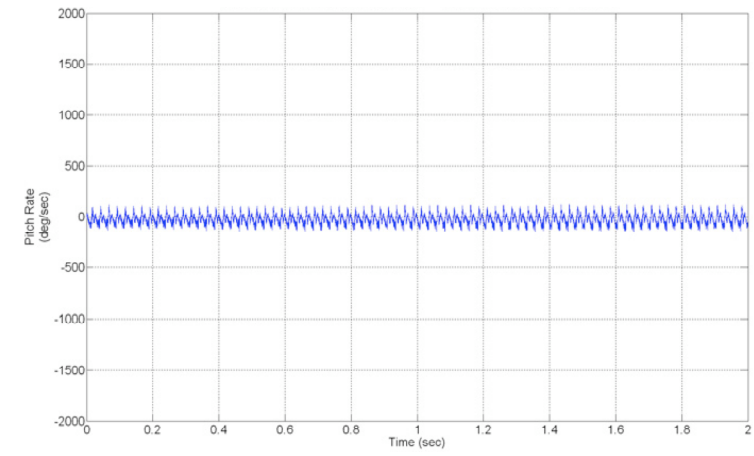
with a lightweight, precise geartrain, and a frictionless magnetic feedback system. To increase the precision of the servo actuation, the feedback sensor system was mounted on the actual hinge axis of the control structure being moved, which reduced the positioning error. Taking that approach to the next level the servo itself was then integrated into the control mechanism, completely removing any control linkage between the servo and the structure being actuated. Using these design techniques, sufficiently light, low power, fast, precise, and durable servo actuators were designed and fabricated for the pitch, roll, and yaw controls, as shown in Fig. 49.

The avionics and servo systems used two different voltages, both lower than that of the three cell series lithium polymer battery pack, which generated between 7.9 Volts and 12.4 Volts depending on charge. Initially, simple linear regulators were utilized because of their simplicity and ease of integration. As the program endurance milestones became increasingly challenging, it became necessary to consider efficient DC to DC power conversion. Custom circuits were developed using the most appropriate COTS integrated circuits, which resulted in significant power conversion efficiency improvements. The avionics power conversion efficiency averaged over a flight increased from 47% to 78%. The main propulsion motor is a DC brushed electric motor which is speed modulated to vary the flapping rate using a simple voltage chopper circuit. Through careful bench testing and design optimization the combined motor and chopper circuit efficiency was increased from 63% to 68% without adding additional weight. To aid in the analysis of power losses of the NAV in flight, power measuring circuits were added to several of the later prototypes. Both battery measurements, and current measurements circuits were installed to allow data logging of the electrical power into the propulsion motor speed controller, and also the servo power supply.

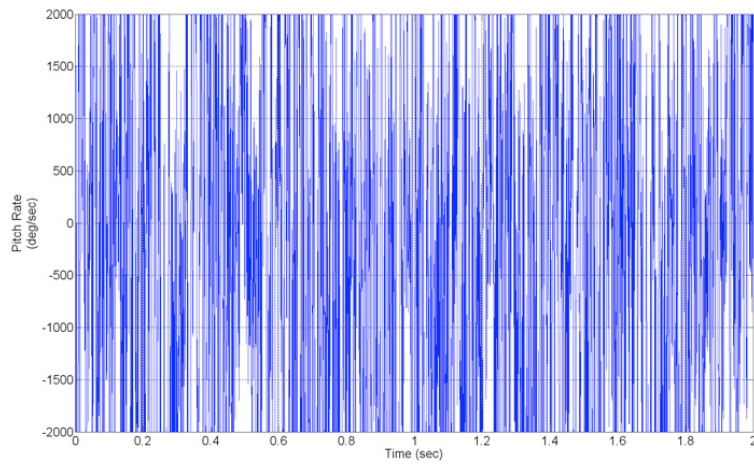
Onboard video is provided by a low resolution analog color CMOS video camera. Video is transmitted to the ground station by a 2.4 GHz FM downlink transmitter. The combined mass of the camera and transmitter is 0.61g.

E. System Modeling and Analysis

As the Nano Hummingbird program progressed, it became apparent that simultaneously meeting wingspan and endurance goals would be very difficult, and the desire to have a vehicle that could realize endurances upwards of five minutes was more important than meeting the 7.5 cm size requirement. The Nano multi-disciplinary design optimization tool was created to address the tradeoffs, primarily between wingspan and endurance. It was conceived as a sizing tool that would also act as an optimizer of the design where possible. Models were developed that were

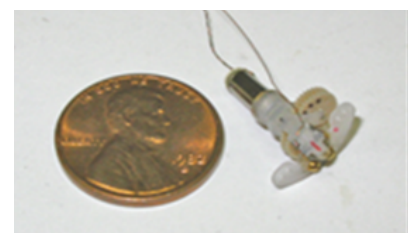


a)



b)

Figure 48. MEMS gyroscope vibration tolerance tests.
Gyroscopes from two different manufacturers mounted identically and logged simultaneously.



a)



b)

Figure 49. NAV Servos. (a) Servo used on early prototypes. (b) Motors for pitch and roll control on Jupiter and Saturn prototypes.

relatively simple in fidelity, yet designed to be backed up by sets of systematically gathered data from existing hardware including batteries, motors, flapping mechanisms, and wings.

One of the most daunting challenges was to develop a model that captured the parametric effects of wing design on performance. It proved difficult because aside from the unsteady aerodynamic effects, small changes in wing design such as batten placement or material variation changed the kinematic behavior of the wings, subsequently altering the aerodynamic performance.

To have a working model that would help the sizing process, it was decided to use a simplified aerodynamic model, backed by extensive experimental data. A baseline wing design was selected, one which had continually proven to be of good performance and durability, which would be parametrically characterized. The goal was to capture the effects of the fundamental geometry, and so a matrix of span, chord, taper was tested (see for example Fig. 19 in section on experimental wing design).

Composing the geometry into a thrust weighted solidity, the resulting data lent itself well to first order helicopter performance models, where the average thrust and power performance are defined by the rotor geometry (solidity, radius, swept area), aerodynamic characteristics (average lift coefficient, airfoil drag, and an induced loss parameter), and the operating conditions (air density, and flapping frequency). Based on our experimental data, the wings' aerodynamic characteristics were determined for this baseline wing to be nearly constant for the geometries and operating conditions tested.

Characterizing the flapping mechanism was also a challenging task (see section on *Flapping Mechanism Performance*). Results of testing indicated that the losses measured in the vacuum could be related to a simple physical model relating the flapping frequency and angular inertia of the wing (see Fig. 33 in section on *Flapping Mechanism Performance*). Consequently, a mass build up model was also created and verified through testing which related the wing planform geometry to the inertia of the wing for a baseline type wing.

The remaining components of the propulsion system, all COTS components, were also tested and characterized. A micro sized dynamometer and power analyzer was used for testing of motors, both brushed and brushless. An analytical model was fit to the test data and related input voltage and current to output torque and speed. Lithium polymer batteries were characterized through discharge tests. Battery mass was also correlated to nominal energy capacity in a linearized equation which allowed a continuous optimization of battery size – this allowed hypothetical scenarios, and the nearest COTS battery sizes could always be examined for performance. Finally, the electronic speed controller was characterized by testing efficiency at a fixed input power but varying throttle setting, with the result fit linearly.

The component analysis modules were combined in a common computational environment. The structure of the system analysis is displayed in Fig. 50, which shows the arrangement of the analysis modules discussed here along with the design variables available for independent continuous control. A gradient based optimizer was wrapped around the system analysis and given control of the design variables in order to optimize a given metric.

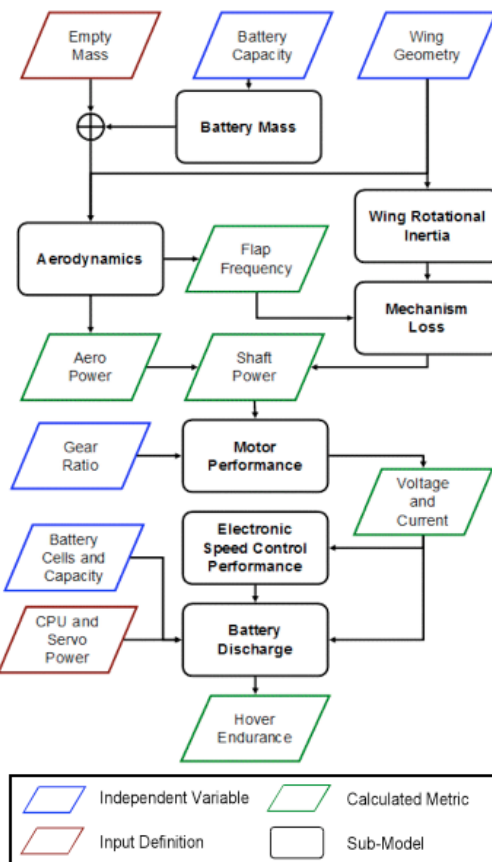


Figure 50: Integrated NAV system analysis structure. This structure was wrapped with a gradient based optimizer to seek solutions to system optimization problems.

Throughout the program, the MDO tool was used for various purposes including:

- “NAV Calculator” - A general use tool for determining and keeping track of component operating conditions – forces and torques on components, RPM, flap frequency, voltage and current, etc.
- Vehicle Sizing – A tool for predicting the battery and wing size to achieve program milestone endurance goals.
- System Impact and Studies – assess the system impact of proposed components prior to integration (e.g. COTS motors, bench tested string drive, addition of video payload and hummingbird body).
- Sensitivity Studies - Build parametric visualization of vehicle sensitivity to variables of interest.
- Design Optimization – limited to determination of optimal gearbox ratio and wing solidity.

In conclusion, the system analysis and optimization environment proved to be a useful tool to aid in the design process and provide vehicle sizing outlooks. But, it had limitations as a tool for optimization of the detailed design. Factors attributing to this limitation include first the challenges of deriving detailed and reliable models of the flapping wing aerodynamics, wing structure deformation, and flapping mechanism performance. Additionally, new and novel subsystems progressed and evolved quickly, for example as the design transitioned from the linkage driven mechanism to the string drive. With these fast paced changes, it would prove difficult for the models to keep current and more importantly act as predictive tools for the purposes of design optimization.

IV. Comparison to Nature

Because the hummingbird was used as the biological model for the AeroVironment NAV, it is interesting to consider a comparison between the two. The decision to emulate a hummingbird in appearance derived from DARPA's desire for the NAV to offer some form of natural stealth by mimicry. However, the desire to emulate the appearance and flight characteristics of a hummingbird does not necessarily require all aspects of the hummingbird to be copied directly. Indeed, some characteristics of the biological hummingbird found their way into the NAV, such as the capability to sustain precision hover without the use of a large tail, while other characteristics such as a figure-eight wing trajectory were not copied in the NAV. Fundamentally, the biological hummingbird and the electromechanical NAV have different constraints. For example, the hummingbird has to do a number of things that the NAV does not, including feeding, sleeping and evading predators, while the NAV is asked to do things a hummingbird is not, such as transmitting realtime video. Available technologies also differ significantly between the two, such as muscles in the case of the hummingbird, and rotary actuators in the case of the NAV. The NAV program was a careful application of the most appropriate technologies to achieve a high level of similarity in appearance and flight characteristics to a biological hummingbird.

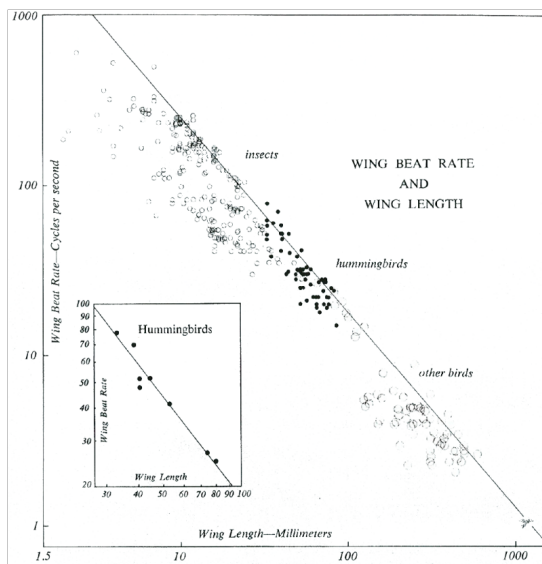


Figure 51. Flapping frequency vs. wing length of biological hummingbirds. (Figure from Greenewalt¹¹)

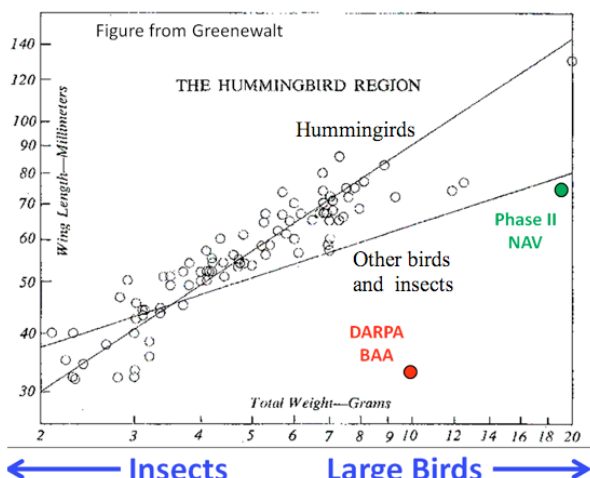


Figure 52. Comparison of wing length vs. weight for biological hummingbirds, initial DARPA NAV requirements (BAA), and final Nano Hummingbird prototype. (Figure from Greenewalt¹¹)

The final NAV prototype aircraft has a mass of approximately 19 g, with the hummingbird-shaped body fairing, video camera and downlink transmitter. The wing span is 16.5 cm, and the flapping frequency in hovering flight is approximately 30 Hz. For comparison, these values are plotted alongside those of biological hummingbirds and the original DARPA NAV requirements in Fig. 51 and Fig. 52. It can be seen that the NAV falls within the range of biological hummingbirds in both wingspan and weight, but its weight per wing length is significantly higher than most hummingbirds, and in fact falls closer to the trend line associated with insects. The original DARPA requirement called for a vehicle with an even higher loading, falling well below even the insect trend line. The NAV flapping frequency at 30 Hz is slightly higher than the value predicted by the trend line for biological hummingbirds of the equal wing length.

V. Conclusion

The NAV program has demonstrated that sustained precision hovering flight with a tailless flapping wing micro air vehicle can be achieved using current technology. In response to the DARPA request for a vehicle unlike any flown in the past, a four and a half year research and development program was undertaken at AeroVironment, culminating in numerous flight demonstrations of hovering flapping wing vehicles. Using the hummingbird as a biological model, the primary focus of the development program was on designing the flapping wing propulsion system and the associated control mechanisms required for tailless flapping wing flight with the capability of precision hover. The problem was approached by building up the system in small evolutionary steps, with extensive use of prototyping and flight testing, complemented by software tools for aerodynamics and MDO.

Control in the pitch, roll and yaw axes was shown to be possible with minimal coupling through combined manipulation of wing pitch by allowing rotation of the wing as a whole, and twist distribution by increasing or decreasing the slack in passively deforming wing membranes. Mechanical solutions equivalent in functionality to the helicopter swashplate have been devised to allow periodic control inputs to the flapping wing system at the flap rate using actuators with bandwidth significantly lower than the flap frequency.

It has been demonstrated experimentally that COTS microcontroller and MEMS rate gyroscope technology are adequate for stability augmentation and remote control of an inherently unstable flapping wing micro air vehicle. Although it was found that some MEMS gyroscopes were unable to tolerate the vibration environment on a flapping wing micro air vehicle, others were found to be suitable.

Concerning the propulsion system, it is critical that the wings and the flapping mechanism be designed as a system, rather than independent components. Efficiency of the propulsion system was found to be strongly influenced by both the losses in the flapping mechanism and the behavior of the wing at the stroke reversals. Reality favored wings capable of higher thrust output at lower flap frequencies, which reduced mechanism losses. Combinations of wing designs and stroke velocity profiles that resulted in the minimum fraction of the flap stroke being traversed during wing membrane camber reversal tended to show the highest performance.

One challenge associated with using computational wing design tools which do not also design the wing structure, is that it is difficult to build a wing that will deform to a prescribed time-varying geometry under flight loads. In the case of the AeroVironment NAV wing design, this problem was approached experimentally. An effective tool to guide the mechanical design of a wing to passively achieve a desired geometry profile in flight would have been very valuable in the development program.

Although the Nano Hummingbird represents a large advancement in the state of the art for flapping wing micro air vehicles, a significant amount of work remains to be done, before the system will be capable of performing a useful mission. In order for the system to be used effectively, the difficulty of piloting the NAV must be reduced significantly from its current level, which is comparable to a stable, model helicopter. The vehicle must also be reliably flyable "heads-down" - through video only when out of visual and audible range. This may be accomplished by utilizing additional sensors such as accelerometers, magnetometers, and an absolute pressure sensor for altitude sensing. Fusion of the data from these sensors will allow for the vehicle's state to be estimated, and its attitude and altitude to be managed automatically, requiring the pilot to give only higher level control inputs. Additional capability for navigation and obstacle avoidance would also be highly desirable. Such capabilities may come from the addition of GPS for outdoor missions, or vision-based technologies for indoor missions.

Increased flight endurance is desirable for use in military, commercial, or other missions. In the absence of a significant advance in battery technology, the largest endurance improvements on the NAV are most likely to come from further reductions in mass of the vehicle, while it is expected that more modest improvements may also come from improved wing and flapping mechanism efficiency.

Resources were not available in the first two phases of the NAV program to address the topic of communications to a level that would be adequate for military, commercial or other missions. Future work would need to focus on

the development of low-power systems capable of providing the NAV with a reliable link to the ground station, having a useful range and the capability to operate in urban environments.

While the Nano Hummingbird appearance is already convincingly similar to a hummingbird in flight, the natural stealth aspects of the vehicle have room for improvement. Most of the effort in the program to the present time has focused on visual stealth. The sound created by the Nano Hummingbird vehicle in flight is still significantly more noticeable than a biological hummingbird. Further development of methods to reduce the creation of noise at the wing stroke reversals is necessary to bring the acoustics of the vehicle to a point where the system would be useful in a covert mission. Further miniaturization of the vehicle as a whole would also improve visual stealth by making it more similar in size to a typical hummingbird or large insect, rather than the largest of hummingbirds as it appears currently. The approach to miniaturization would likely include further refinement of the mechanism designs and fabrication techniques, with an additional focus on weight reduction of the entire vehicle.

Acknowledgments

This work was sponsored by the Defense Advanced Research Projects Agency (DARPA) under contract W31P4Q-06-C-0435. We are grateful to Todd Hylton, John Main, and Darryll Pines, who served as the Nano Air Vehicle program managers. We would also like to thank Vince Castelli, Christopher Martin, Matt Maroofi, Bill McBride, Ray Morgan, Kevin Pick, and Richmon Tun, who provided the government with critical scientific, technical and engineering review, as well as interface between the government managers and the contractors. The authors would also like to acknowledge all of the contributors to the project at AeroVironment: Peter Zwaan, Bart Hibbs, Ben Pipenberg, Brian Daniels, Dave Saks, Shanling Yang, Roger Schuck, Glenn Blevins, Reza Miremadi, Mark Levoe, Jenny Dao, Linda Garcia, Dana Taylor, Michael Simpson, Erik Steltz, Paul MacCready, Lars Cremeann, Bruce Benton, Jim Hodge, George Lacour, Rick James, William Lott, Nate Hopkins, and Justin McAllister. We would like to thank our technical partners from Phase 1 of the program: Kenneth Hall of Duke University, Michael Selig of the University of Illinois at Urbana-Champaign, Geoffrey Barrows of Centeye, Inc., Mario Munich of Evolution Robotics, and Stewart Clark of Irvine Sensors.

References

- ¹Defense Advanced Research Projects Agency (DARPA), *BAA 06-06 Proposer Information Pamphlet: Nano Air Vehicle (NAV) Program*, Washington D.C.: Defense Sciences Office, 2005, on-line, available at URL: <https://www.fbo.gov/spg/ODA/DARPA/CMO/BAA06-06/listing.html>
- ²Zdunich, P. et al., "Development and Testing of the Mentor Flapping-Wing Micro Air Vehicle," *Journal of Aircraft*, Vol. 44, No. 5, 2007, pp. 1701-1711.
- ³Lentink, D., Jongerius, S.R., and Bradshaw, N.L., "The Scalable Design of Flapping Micro-Air Vehicles Inspired by Insect Flight", *Control*, Springer-Verlag, Berlin, 2009, Chapter 14, pp. 185-205
- ⁴Brooks, A. N., MacCready, P. B., Lissaman, P. B. S., and Morgan, W. R., "Development of a Wing-Flapping Flying Replica of the Largest Pterosaur," *AIAA/SAE/ASME/ASEE 21st Joint Propulsion Conference*, Monterey, CA, July 1985, AIAA Paper 85-1446
- ⁵Keenon, M. T., and Grasmeyer, J. M., "Development of the Black Widow and Microbat MAVs and a Vision of the Future of MAV Design," *AIAA International Air and Space Symposium and Exposition: The Next 100 Years*, Dayton, OH, July 2003
- ⁶Hall, K. C. and Hall, S. R., "Minimum Induced Power Requirements for Flapping Flight," *Journal of Fluid Mechanics*, Vol. 323, 1996, pp. 285-315.
- ⁷Hall, K. C., Pigott, S. A., and Hall, S. R., "Power Requirements for Large-Amplitude Flapping Flight," *Journal of Aircraft*, Vol. 35, 1998, pp. 352-361.
- ⁸Hall, K. C. and Hall, S. R., "A Rational Engineering Analysis of the Efficiency of Flapping Flight," in *Fixed and Flapping Wing Aerodynamics for Micro Air Vehicle Applications*, Vol. 195, T.J. Mueller, Ed.: AIAA, Reston, VA, 2001, pp. 249-274.
- ⁹Lebental, S., "Optimization of the Aerodynamics of Small-Scale Flapping Aircraft in Hover," Ph.D. Dissertation, Mechanical Engineering Dept., Duke Univ., Durham, NC, 2008.

¹⁰Drela, M., "XFOIL: An Analysis and Design System for Low Reynolds Number Airfoils," *Low Reynolds Number Aerodynamics*, Springer-Verlag Lecture Notes in Engineering, edited by T.J. Mueller, No. 54, Springer-Verlag, Berlin, 1989

¹¹Greenewalt, C.H., *Hummingbirds*, Dover Publications, New York, 1990, Chapter 3, pp. 123-125